Soft Matter

www.softmatter.org

Volume 4 | Number 10 | 1 October 2008 | Pages 1925–2112

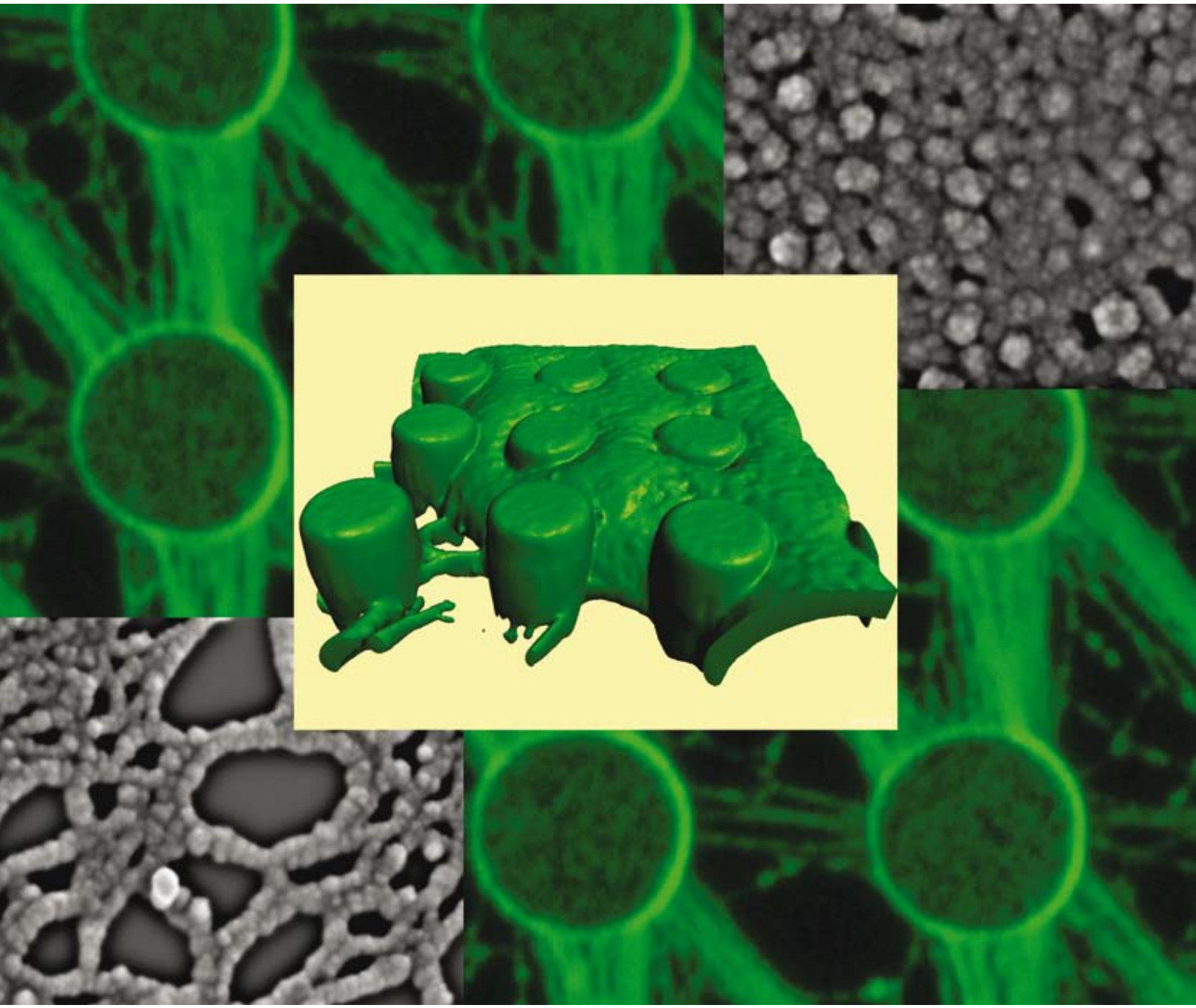

ISSN 1744-683X

RSC Publishing

Force-induced fibronectin fibrillogenesis *in vitro*†

Jens Ulmer,[abc] Benjamin Geiger[c] and Joachim P. Spatz*[ab]

Received 12th May 2008, Accepted 17th June 2008
First published as an Advance Article on the web 12th August 2008
DOI: 10.1039/b808020h

Polymerization of fibronectin (FN) and its assembly into fibers, *in vitro*, is a two-step self-assembly process, initiated by the formation of a stable FN sheet made of globular particles at the air–liquid interface, and followed by shear-force driven fibrillogenesis along a superhydrophobic surface made of elastic micropillars. The initially-formed fibrils, displaying "rough" surfaces with globular subdomains, can be further stretched into "smooth" fibers with a characteristic diameter of 14 nm. Using high-resolution scanning electron microscopy, we demonstrated that the fibers formed *in vitro* are highly similar to an FN matrix produced by cultured fibroblasts. Furthermore, we showed that the stretched FN fibrils can support cell adhesion, and display antigenic epitopes which appear to be sequestered in the relaxed molecules. These findings suggest that cells are able to mechanically fine-tune the biological activity of the underlying matrix by modulating its structure, surface properties and organization.

Introduction

The extracellular matrix (ECM) is composed of diverse classes of adhesive and scaffolding molecules which form a rich variety of filamentous networks with distinct physical and chemical properties.[1,2] Concertedly, these ECM fibers play key roles in tissue scaffolding[1] and in adhesion-mediated signalling processes,[3] both mediated *via* specialized adhesion receptors, mostly integrins.[4,5] Consequently, these interactions affect multiple cellular responses, including the regulation of cell survival, differentiation, proliferation and migration.[6] However, despite their crucial physiological importance, the mechanisms underlying signalling by cell–ECM adhesion are still unclear.

Recent studies indicate that multiple processes act together to modulate ECM structure and function. These include the expression and secretion of ECM components,[1] regulated cross-linking of the ECM, which affects its structure and mechanical properties,[1,7] degradation of the matrix by cell-associated, membrane-bound enzymes,[8,9] and mechanical-force-induced matrix rearrangement.[2,5,10–12]

FN is one of the most abundant glycoproteins in the ECM. This large, homodimeric protein consists of polypeptides of *ca.* 235 kDa each, covalently linked to each other *via* two disulfide-bonds located near their C-termini.[13] Each polypeptide chain comprises a linear array of three types of repeats, known as FN-I, FN-II, and FN-III modules. These domains are characterized by repeating units whose three-dimensional structure is well-characterized: type I and type II modules are compact disulfide-bonded structures, whereas type III repeats, which comprise more than half of the protein, exhibit a seven-β-stranded sandwich motif, resembling, in overall structure, immunoglobolin-(Ig-)domains.

FN exists either as a soluble protein produced by hepatocytes and released into the blood, or as a fibrous ECM protein.[14] In its soluble form, FN is important for blood clot formation;[15] in the ECM, it functions as a multi-domain adhesive protein that can bind to a variety of partner ECM molecules, including collagen, heparin and fibrin, as well as to specific cell surface integrin receptors.[6,16] Apart from cell adhesion, the FN-based matrix regulates cell migration, differentiation, and growth, both in adult tissue and during embryonic development.[17] Loss of FN from the cell surface is a characteristic property of many malignant cells, and restoration of the FN matrix can affect the malignant phenotype.[18]

A characteristic feature of FN is its capacity to form fibrillar networks.[15] FN fibrillogenesis depends on specific self-binding sites, such as repeats 2–5 in the FN-III domain and in the FN-I domain, close to the N-terminus.[14,19,20] Baneyx and Vogel [21] observed aggregation and fibrillogenesis of FN upon adsorption to a water-suspended lipid monolayer and showed that these processes were accompanied by substantial deformation of FN's original globular structure. Moreover, it was shown in cell cultures that the development of mechanical tension is necessary for efficient FN fibrillogenesis.[22–25] These studies indicated that FN exists in a stretched conformation in fibrils, and in a "relaxed" conformation on the cell surface or in solution, and

[a]*Max Planck Institute for Metals Research, Department of New Materials and Biosystems, Heisenbergstr. 3, D-70569 Stuttgart, Germany. E-mail: spatz@mf.mpg.de*
[b]*University of Heidelberg, Department of Biophysical Chemistry, Germany*
[c]*Department of Molecular Cell Biology, Weizmann Institute of Science, Rehovot 76100, Israel. E-mail: benny.geiger@weizmann.ac.il*

† Electronic supplementary information (ESI) available: S1: movie indicating the bending of the micropillars when the air–fibronectin solution interface moved within the microstructure. This enables the estimation of the force generated during the wetting process, based on the deflection of the pillars. These measurements indicated an average force of 180 ± 36 nN per pillar. S2: movie indicating the bending of the micropillars when the air–BSA solution interface moved within the microstructure. In the case of BSA, a sheet-to-fiber transition did not occur; rather, the free, suspended BSA sheet became fragmented and collapsed without forming fibrillar structures. S3: movie indicating the bending of the micropillars when a PBS droplet not containing FN is wetting the micropillar interfaces. This resulted in substantially stronger bending of the pillars than that which occurred when FN was dissolved in the PBS droplet. Analysis of the pillar movement indicated that the force driving the bending of pillars, produced by PBS alone, was 279 nN ± 46 nN. See DOI: 10.1039/b808020h

that, indeed, conformational changes occur during cell-induced FN aggregation and stretching.

Two different mechanisms which could account for the formation of FN fibers and for the fiber's elasticity are presented in the literature. Erickson's model[12,26] proposes that FN molecules in relaxed fibers are bent and looped into a compact quaternary conformation. Stretching the fibers pulls the molecules into the extended conformation; however, the domains themselves remain folded. This model postulates the mediation of FN molecules *via* their N-terminal binding sites while the protein still retains a compact globular conformation, which is reinforced by electrostatic intra-chain interactions between FN-III domains 2–3, and 12–13. Vogel and co-workers' model[25,27] suggests that the molecules in the fibrils are already extended, and that elastic stretching is produced by force-induced unfolding of FN type III domains. In both models, it is assumed that the longitudinal connection of adjacent FN molecules involves bonds between the respective N-terminal FN-I domains. Forces needed for unfolding the compact globular conformation, reinforced by electrostatic intra-chain interactions, were measured at less than 5 pN,[28,29] while forces needed for unfolding FN-III domains were calculated to be more than 10 pN.[30]

In order to distinguish between the different models, it is necessary to measure the elasticity per molecule in FN fibers, and visualize their structure as a function of applied force. The force required for unfolding the type III module is surprisingly small, comparable to the mechanical force generated by several myosin motors.[28] Indeed, it is believed that the forces applied to FN at the cell–matrix interface are primarily generated by the contractile actomyosin-based cytoskeletal machinery, which is transmitted to the ECM *via* focal adhesions (FAs) and related integrin-mediated contacts.[4,31] These adhesions were shown to be highly mechanosensitive, namely, they grow when subjected to local mechanical stress, and shrink when the tension decreases.[32] Thus, mechanical forces appear to affect cell–ECM adhesions in several ways, regulating both the assembly of integrin adhesions and the structure of the underlying FN matrix.[5]

Results and discussion

Confocal microscopy studies of droplets (20 μL) containing fluorescently labeled FN in PBS (10 μg mL^{-1}) and aliquoted onto flat PDMS surfaces indicated that within minutes of aliquoting, the fluorescently tagged FN partitioned to the air–liquid interface, forming a uniform protein shell (Fig. 1a). Accumulation at the air–water interface is, however, not unique to FN, and was also observed with other proteins, such as Bovinum Serum Albumin (BSA) and IgG (data not shown). The partitioning of FN to the air–liquid interface was accompanied by a consistent decrease in the contact angle between the PDMS surface and the protein-containing droplet. After 20 min of incubation, the translocation of FN to the droplet periphery reached a plateau: the contact angle with the PDMS surface dropped from 75° to 65° for a 10 μg mL^{-1} solution (Fig. 1a), and from 60° to 50° for a 100 μg mL^{-1} FN solution (data not shown). In comparison, the contact angle of pure water on PDMS is *ca.* 110°.[33]

To examine the dynamic properties of the FN shell at the air–water interface, the rate of fluorescence recovery after photobleaching (FRAP) was measured at the droplet periphery. Fig. 1b shows confocal fluorescence micrographs displaying the recovery of FN fluorescence at different time points following photobleaching. Fluorescence monitoring was performed within the black (bleached) square area, denoted by a star. At the outermost, original interface, which was formed 1 h before

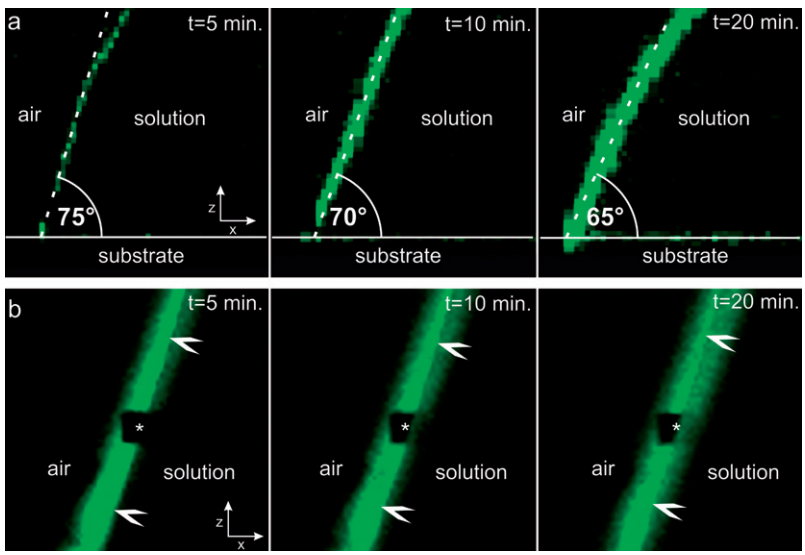

Fig. 1 The formation of an immobile FN "shell" at liquid–air interfaces. (a) Fluorescent confocal microscopy images of a drop containing pre-labeled FN (10 μg mL^{-1}) in contact with a flat PDMS substrate, recorded 5, 10 and 20 min after aliquoting the drop onto the PDMS surface. The images show time-dependent changes in the contact angle and an increase in fluorescence at the air–solution interface. (b) Time series of confocal fluorescence micrographs, displaying the protein exchange dynamics at the air–solution interface after photobleaching. Dye bleaching was initiated 1 h after injecting FN into the droplet, and was followed by injecting fresh FN into the droplet. The original protein border, which formed after 1 h, is indicated by the white arrowheads. Fluorescence recovery after photobleaching was measured in the area denoted with a star. While fresh FN readily interacted with the bleached zone, the original interface essentially did not recover during the 20 min timeframe of this experiment.

bleaching, the extent and rate of recovery depended on the choice of protein. Fluorescence recovery was 65% for FN and 60% for BSA, measured approx. 20 min after bleaching with no further significant increase. In contrast, IgG showed a higher maximal fluorescent recovery of 90% after 20 min, suggesting weaker aggregation and higher mobility of IgG molecules at the air–water interface compared to FN or BSA.[34] Injection of additional fluorescent protein into the droplet after 1 h resulted in instantaneous accretion of protein to the interface layer (Fig. 1b; the original border of the protein shell is indicated by white arrowheads). Immediate bleaching of the freshly aggregated FN showed that the recruitment of molecules to the inner aspect of the FN shell persisted normally, resulting in ~100% recovery after 20 min (Fig. 1b).

To compare the mechanical properties of FN to those of BSA and IgG at the air–liquid interface, small droplets of *ca.* 50 μL, each containing 10 μg mL^{-1} of one of these proteins, were applied to the tops of hydrophobic PDMS micropillars (diameter 5 μm, height 10 μm, separated from each other by 4 μm). Examination of 3D confocal images indicated that the protein-containing droplets remain suspended on the micropillar tops, exhibiting a nearly spherical shape, with a contact angle of liquid against the micropillar surfaces of nearly 180° (a phenomenon known as "superhydrophobicity").[35] Gentle replacement of the FN- or BSA-containing drops with fresh, protein-free buffer resulted in the deposition of a thin, 2D protein layer on the tops of the pillars, bridging the space between adjacent pillars (Fig. 2a and b, top right corner, for FN; Fig. 2c and d for BSA).

Application of 100 μL of a 0.5% (v/v) polyvinyl alcohol (PVA) solution in PBS led to a decrease in the surface tension of the suspended FN solution, enabling the solution to penetrate into the interpillar space, rather than remaining suspended on the pillar tops. In Fig. 2a and b, this "wetting transition" was monitored by confocal microscopy. The white arrowheads indicate the transition line between the continuous protein layer, still suspended on the tops of the pillars, and a fibrous network formed in areas where the interpillar space was completely wetted (see left bottom corners of Fig. 2a and b). As the air–solution interface moved within the microstructure, the elastic pillars bent (ESI, Movie S1†), enabling the estimation of the force generated during the wetting process, based on the deflection of the pillars. These measurements indicated an average force of 180 ± 36 nN per pillar.[36,37] Obviously, this mechanical force strongly affects FN organization, as visualized at different states of wetting. The force applied to the protein sheet is a result of local bending of micropillars due to the wetting of the micropillar field. Non-wetted areas are stabilized by non-bended pillars which also indicate that no force is propagated across the pillars to the non-wetted areas.

The 3D image reconstruction of the transition area unravels the force-induced reorganization of the interface-associated FN in the interpillar space (Fig. 2b). As mentioned above, the pillar heads bent during this movement, indicating a substantial amount of force acting on the FN sheet. As a consequence, the continuous FN layer transformed into discrete fibrils, bridging between adjacent pillars. Identical results were obtained by pulling the drop of FN solution laterally toward the micropillar interface, indicating that the addition of PVA *per se* has no effect on FN organization (data not shown). It is noteworthy that the

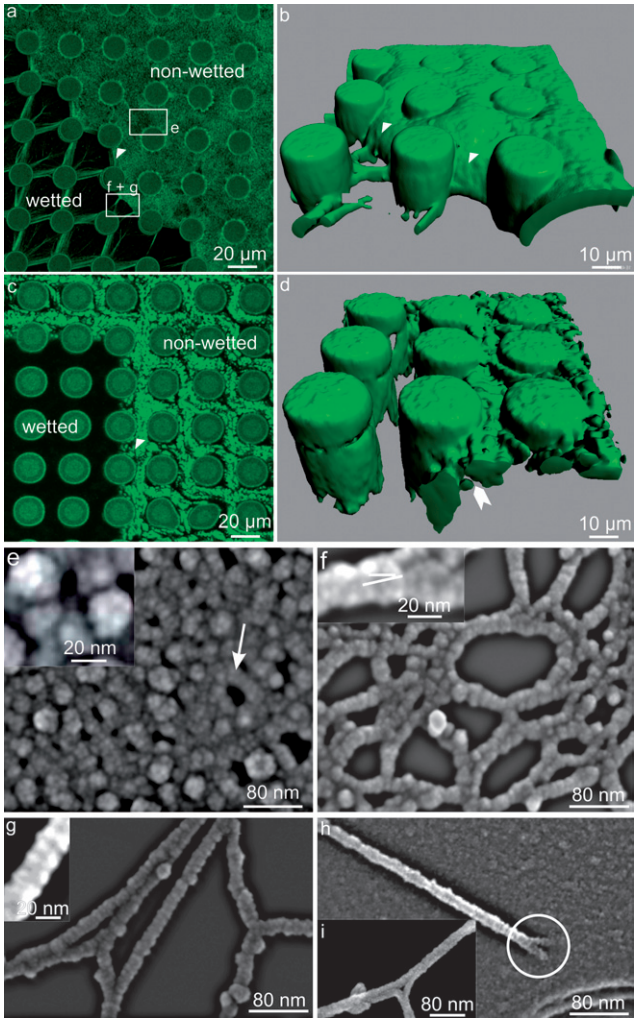

Fig. 2 Fluorescence microscopy and high-resolution SEM images depicting FN fibrillogenesis on micropillar arrays. (a) Confocal fluorescent micrograph of a sample, chemically fixed during the wetting process of a micropillar interface after a thin layer of FN was partitioned into the air–solution interface, showing the tendency of FN to generate fibrils during the wetting of the microstructured surface. The non-wetted micropillar area (top right) displays a thin layer of protein associated with the pillar tops. The reconstruction of 3D confocal fluorescence micrographs in (b) indicates that the pillars are bent (white arrowheads). The border between the wetted and non-wetted interface extends from the upper left to the lower right area. Under non-wetted conditions, fluorescent confocal images of BSA layers also indicate the accumulation of a thin protein film at the air–water interface, spanning the area between the pillars; no fiber formation was observed upon wetting of the surface [arrows, (c) and (d)]. Instead, the protein layer disintegrated into small fragments upon wetting of the micropillars. Panels (e), (f) and (g) show SEM micrographs, revealing FN structures from regions represented by the areas in (a) (bordered in white). All SEM images were obtained following critical point-drying and 2 nm thick chromium coating. Note that in the fibrilar structures globular subdomains remain visible [insets (f) and (g)]. (h) The thinnest fibers observed had diameters of *ca.* 14 nm, and exhibited a smooth surface. The end of an individual 14 nm thick fiber (white circle) displayed two *ca.* 7 nm wide subfibers, which most likely correspond to two dimeric FN molecules associated with one individual fiber. (i) Thicker fibers were formed from the lateral assembly of individual 14 nm thick fibers.

integrity of FN is critical for its fibrillogenesis. Western blot analyses of different FN preparations revealed that fragmented FN could not form fibers on the microstructured surfaces when applied in the same manner (data not shown). In the case of BSA, such sheet-to-fiber transition did not occur; rather, the free, suspended BSA sheet became fragmented and collapsed without forming fibrillar structures (Fig. 2c, d, and ESI, Movie S2†).

Initiating the wetting of the micropillar interfaces by a PBS droplet not containing FN, which is suspended on the pillar tops, resulted in substantially stronger bending of the pillars than that which occurred when FN was dissolved in the PBS droplet. Analysis of the pillar movement (ESI, Movie S3†) indicated that the force driving the bending of pillars, produced by PBS alone, was 279 ± 46 nN. Since the forces applied to the microstructures through wetting were assumed to be the same, irrespective of the protein being dissolved in the drop, this greater degree of pillar bending was attributed to the missing connection between the pillars through FN fibrils or sheets which, in the former case, could carry substantial amounts of load.

A more detailed view of the continuous 2D protein sheet, deposited on the micropillar array and spanning the area between micropillar tops, was obtained by high-resolution scanning electron microscopy (hrSEM), revealing a dense mesh of spherical-to-elliptical particles with an apparent mean diameter of 32 nm (Fig. 2e). This is in general agreement with previous studies, which indicated that soluble FN, in its compact, globular conformation, has an elliptical shape, with dimensions of 51 nm × 32 nm.[38,39] These findings indicate that the formation of globular FN structures is not a consequence of the protein's contact with a hydrophobic PDMS surface, but rather is spontaneously induced upon accumulation of the protein at the droplet–air interface. Notably, all hrSEM measurements were performed on critical point-dried specimens that were coated with an approximately 2 nm thick chromium layer, in order to prevent charging. To avoid confusion, all hrSEM-based values mentioned herein correspond to net values, obtained by subtracting the coat thickness from the measured dimension.

Upon application of force, FN particles became scarce, and the most prominent structures found in the interpillar space were laterally stringed or fully aligned FN fibrils (Fig. 2f–i). The micrographs depict FN fibers that were apparently stretched to differing degrees. Consequently, the structure of the fibers varied, from "rough" fibers displaying a globular sub-structure (Fig. 2f) with a typical diameter of 24 nm, to smooth, stretched fibers with a characteristic diameter of 14 nm (Fig. 2g–i). Detailed analysis of these fibers indicated that the globular domains were elliptic, with dimensions of 24 nm × 16 nm. It is noteworthy that the aspect ratio between the two extensions of elliptically shaped FN molecules observed in solution was similar to that of these subdomains, namely *ca.* 1.6 [38,39] which is an indication of globular structures near in size to those found unstretched in solution. Further stretching of the fibers (Fig. 2g) resulted in the formation of thinner fibers, where globular subdomains of 19 nm × 9 nm dimensions (aspect ratio 2 : 1) were still apparent. The thinnest fibers observed by hrSEM have a diameter of *ca.* 14 nm, with no apparent globular sub-structure (Fig. 2h). At their ends, however, these fibers often split into two parallel fibers, each *ca.* 7 nm thick. Notably, the diameter of a single side-chain of the FN molecule, estimated by transmission EM,[26] is *ca.* 3 nm. As we could not find sub-fibrils with an apparent diameter smaller than 7 nm, we conclude that these thinnest fibrils represent dimers, composed of two laterally aligned FN chains. The dimensions of these FN assemblies are summarized in Table 1.

The patterns of fibers formed on each micropillar matrix were highly regular, though the variations between preparations were usually large. This could be attributed to limited control over the exact wetting process, and the shear stress applied to different preparations. Somewhat better control over the long-range organization of the FN network formed on these surfaces was obtained by applying uniform shear stress to FN droplets, without liquid wetting of the entire interface. Thus, the specific fibrillar FN patterns formed on the micropillar arrays can be affected by multiple factors, including FN concentration, incubation time, and force direction. For example, concentrated FN solutions (100 μg mL^{-1}) usually yielded thick bundles of FN fibers connecting adjacent pillars, and flanked by finer meshwork interconnecting these bundles (Fig. 3a). Lower concentrations (10 μg mL^{-1}) of FN yielded networks dominated by thin bundles running between the micropillars, with only a few interconnections (Fig. 3b). Wetting or changing droplet pulling speed also

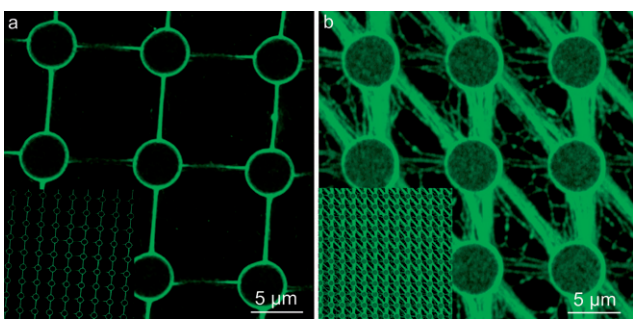

Fig. 3 The effect of FN concentration on the assembly of FN arrays. Confocal fluorescent optical micrographs show that FN fiber arrays, deposited on the micropillar interface from droplets containing (a) 10 μg mL^{-1} or (b) 100 μg mL^{-1} FN are highly regular (see insets). Higher FN concentrations strongly support the formation of thick bundle arrays interconnected by a loose fiber network.

Table 1 Observed FN assemblies and their dimensions

FN assembly geometry	Sheet made of globular particles	Rough fibers with globular subdomains (mild stretching)[a]	Rough fibers with globular subdomains (extensive stretching)[b]	Smooth fibers (full stretching)
Images	Fig. 2e	Fig. 2f	Fig. 2g	Fig. 2h, i
Dimension (∅)	32 nm	24 nm × 16 nm	19 nm × 9 nm	14 nm

[a] The axial dimension of these dimensions is 24 nm. [b] The axial dimension of these dimensions is 19 nm.

affected the FN fibril array. Further attempts to standardize the FN patterns are currently underway.

Initially, the sheet composed of globular FN particles (Fig. 2e) was stabilized by its adhesion to the micropillar tops. Wetting of the micro-interface caused bending of the pillars and application of lateral shear forces to the FN sheet, resulting in the collapsing of the FN sheet and the formation of diverse fibers. Micropillar tops are characterized by a unique property: stretching applied to a 2D FN sheet immobilized onto a pillar top, increases gradually from the center of the pillar top to its edge, perpendicular to the bending direction of the pillars (Fig. 4a, green line). This finding is consistent with the observation that the bending of pillars results in lateral necking of the original homogeneous FN sheet (Fig. 4a, b). Consequently, FN molecules which are not located along the shortest line connecting two adjacent pillar top centers must undergo greater deformation, due to geometric adaptation of the deformed FN sheet (Fig. 4a, b).

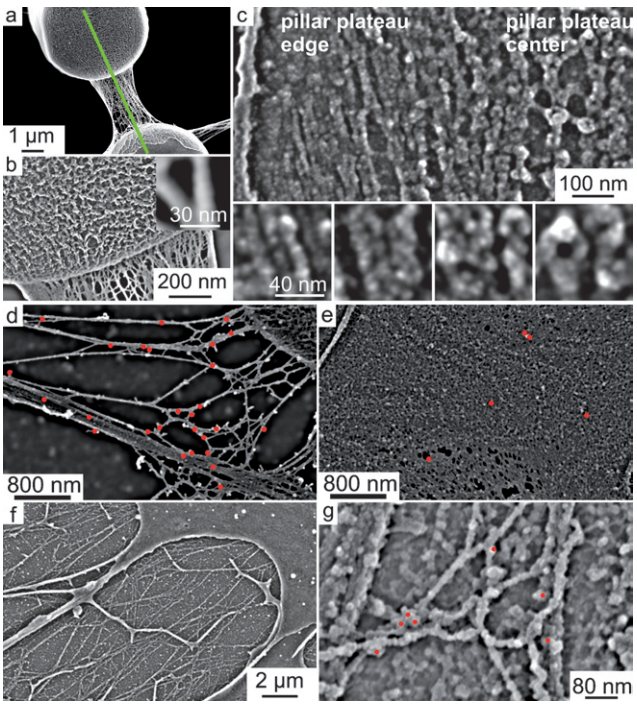

Fig. 4 Ultrastructural analysis of force-induced and cell-produced FN fibrils. (a–c) Ultrastructural analysis, by hrSEM, of the micropillar arrays after FN deposition indicating that discrete fibers are formed on top of the micropillars and in between them. The green line in (a) indicates the pillar bending direction. (c) Presentation of the FN organization on top of a pillar plateau. FN stretching increased from the center to the edge of the pillar plateau. The bottom row of images shows fibers at different stages of unfolding, at higher magnification. The stretching direction is vertical. (d) The FN fibers and (e) sheets of globular FN were labeled with immunogold (marked by red dots). SEM images of immunogold-labeled FN fibrils, formed *in vitro*, indicate a substantially higher degree of antibody binding along FN fibers (d) compared to suspended FN sheets (e). Panels (f) and (g) show SEM images of FN fibers generated *in vivo* by cultivating primary human fibroblasts on non-treated silicon surfaces for 4 d. After critical point-drying and immunogold-labeling, the filaments were imaged at high-resolution, revealing a similar morphology to that found on or in between the micropillars [compare to (d)].

Local variations in the extent of FN stretching results in varying degrees of FN unfolding, detectable by hrSEM. In Fig. 4c, the pulling direction follows a line from the top to the bottom of the image. At the center of the pillar plateau, globular particles originally formed at the air–liquid interface are revealed as doughnut-shaped FN particles with a diameter of *ca.* 36 nm and a toroidal width of 13 nm, partly arranged in strings directed towards the pulling direction. The doughnut-shaped structure defining the corona is approximately 11 nm wide. Hydrophobic interactions between the pillar plateau and globular FN causes partial projection of 3-dimensional FN molecular structures at the interfaces, thereby enabling further resolution of sub-structure unfolding which has been also observed on flat PDMS after deposition of a FN sheet. Nearer to the pillar top edge (where FN stretching increases), the doughnut-like structures are further deformed, and gradually transform into 14 nm fibers, composed of two 7 nm subfibers.

In order to examine the molecular properties and biological relevance of FN fibers stretched to varying degrees *in vitro*, we immunogold-labeled the stretched fibers with FN antibodies (Fig. 4d, e) and compared their labeling to that of a relaxed FN sheet, and to FN fibrils generated by primary cultured fibroblasts (Fig. 4f, g). hrSEM images of the immunogold-labeled FN (denoted by the red dots in Fig. 4g), showed that the force-induced fibrils displayed much more intense immunogold-labeling than the "relaxed" FN particles, suggesting that mechanical stretching of FN fibers exposes cryptic antigenic sites that are not available in its globular conformation. hrSEM images of primary fibroblasts showed that after 4 d in culture, a dense network of ECM fibrils was formed. Using immunogold-labeling for FN, it was shown that these fibrils contained FN (red dots in Fig. 4g). The dimensions of these fibrils were found to be 12 nm and thicker. Remarkably, the intensity of the immunogold-labeling along the cell-produced fibers (Fig. 4g) was considerably lower than that found on the fibers generated *in vitro* (Fig. 4d) suggesting that either the natural fibers are less stretched and, consequently, less unfolded than the fibers formed *in vitro*, or they contain additional proteins that mask or modify their immunoreactivity. It should be noted that the naturally occurring fibrils were far less homogeneous in thickness and overall shape than the ones generated *in vitro*, reflecting their molecular heterogeneity, and local variations in both the protein concentrations of native ECM networks, as well as in the forces applied to the ECM networks by the associated cells.

To measure the tensile strength of the FN fibrils generated *in vitro*, we subjected FN fibers stretched between adjacent micropillars to mechanical stress, using micromanipulation (Fig. 5a). Measurement of the stress–strain relationships indicated that fiber bundles with an approximate diameter of 1 µm show a linear stress–strain relationship for the first 1 µm of deformation (Fig. 5b). These data were obtained from the micromanipulation experiment (Fig. 5c). The position of a rigid microneedle, which deformed a pillar to which a single FN fiber was attached, is indicated by the red line. The movement of the pillar, which was connected *via* a single FN fiber (see arrow) to the pillar on which the force was applied by the microneedle, was recorded by the displacement of the pillar top (white asterisk). The fibers were attached to the side of the pillar about 5 µm below the pillar top. The spring constant of the micropillar was independently

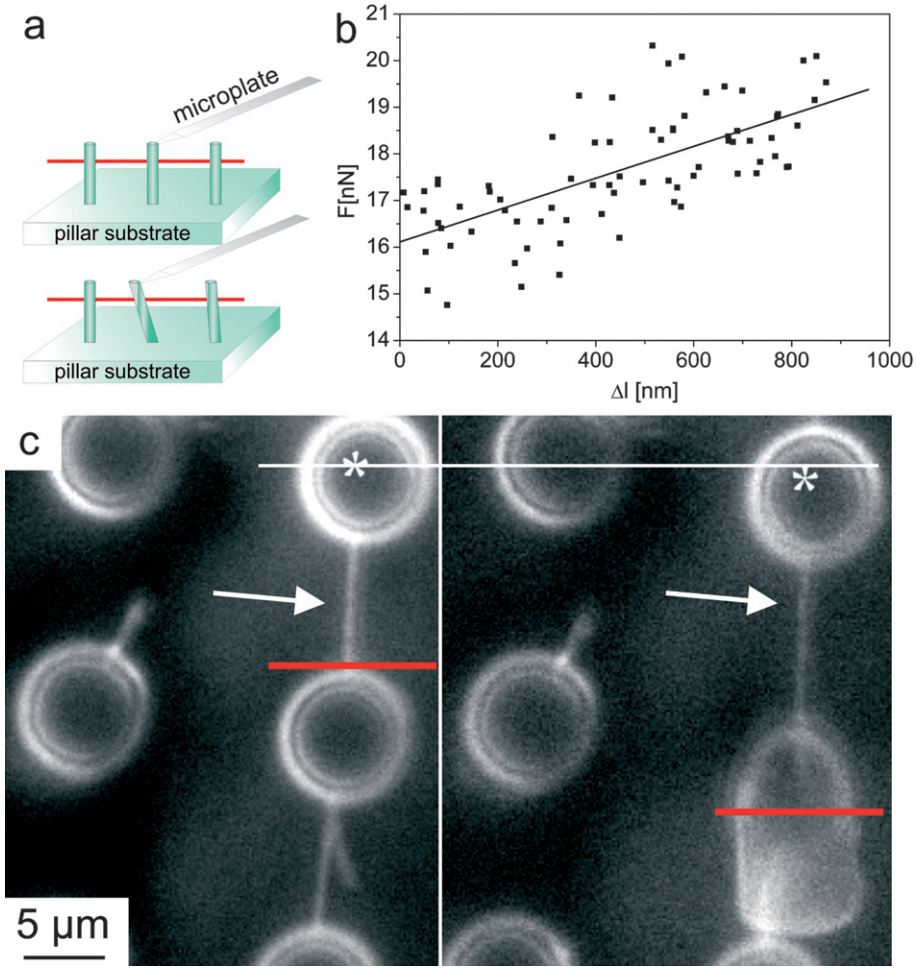

Fig. 5 The stretching of elastic FN fibrils. (a) A schematic drawing of the experimental set-up used to perform the mechanical deformation of a single FN fiber. The rigid microplate is attached to a single pillar head. The pillar is deflected by moving the sample beneath the affixed microplate. Subsequent analysis of the directly connected pillar enables calculation of the fiber's load. (b) The force deformation relation of a single FN fiber with an apparent thickness of approximately 1 μm revealed a stiffness of 3.4 mN m^{-1}. (c) Measuring the mechanical properties of a single FN fiber with flexible PDMS posts by deflecting one pillar with a rigid microneedle (red line). The pillar marked by an asterisk and connected *via* a single FN fiber (arrow) was analysed to calculate the load of the fibril in between the pillars.

measured to be 0.9 N m^{-1}. Thus, the fiber stiffness was calculated to be ~3.4 mN m^{-1}. A substantial load, with no rupture of the fibers was obtained. Furthermore, the fibers always retracted to their original length following release of the force, confirming their elastic character.

Cellular interactions with fibrous FN, and the mechanical interplay between them, were explored by plating rat embryo fibroblasts, stably expressing YFP-tagged paxilin (PAX), on micropillar surfaces containing pre-assembled FN fibrils. After fixation, the cells were further stained for actin and FN and examined by confocal fluorescence microscopy, as shown in Fig. 6 for different fiber geometries. Fig. 6c and f display highly magnified fluorescent images of PAX, FN, and the calculated intensity ratio between them in the marked areas (Fig. 6a, b, d, e). As shown, the cells established FA not only on the FN-coated micropillar tops, but also along the pre-assembled, free-hanging FN fibers. This finding indicated that these fibers could resist forces exerted at FA, which are typically within the range of a few tens of nanonewtons.[31] These forces were, however, strong enough to deform the regular pattern of thin FN fibers with an apparent diameter of less than 1 μm (Fig. 6a, b). On the other hand, cells attached to thicker bundles with a diameter of 2 μm (Fig. 6d, e) oriented themselves along the length of the fibers, while inducing only minor perturbations in the FN fiber geometry. Notably, the projected area of FA directly correlates with the local force applied to the underlying substrate shown in previous studies to be in the range of 5–10 nN per μm^2.[31,36] In our samples, cells did not preferentially form smaller FAs on fibers as compared to the pillar tops, indicating no difference in stiffness between pillar tops and FN fibers. This finding is in agreement with the observation that FN fibers adapt themselves to the mechanical load between pillars, which, however, is in equilibrium with the degree of pillar bending.

The results presented herein demonstrate that FN fibrillogenesis *in vitro* is a two-stage process initiated by the shear-stress independent partitioning of globular FN particles to the air–solution interface where they form an insoluble 2D sheet, followed by force-dependent fibrillogenesis. These

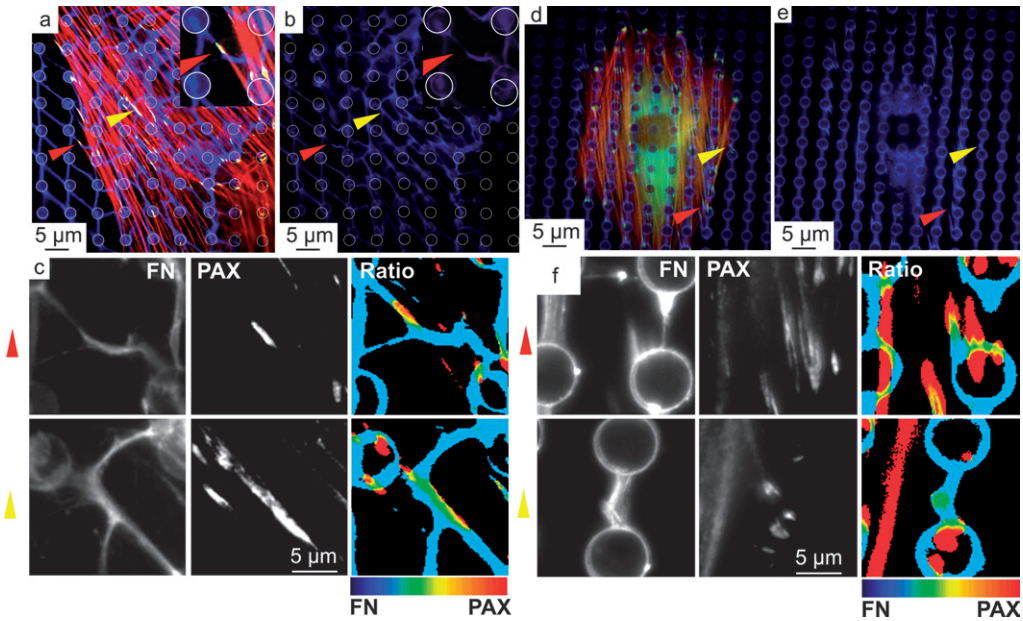

Fig. 6 The interaction of rat embryo fibroblasts with force-induced FN fibrils. Fluorescent optical micrographs illustrate the response of rat embryo fibroblasts growing on artificially-produced FN fibers with various bundle thicknesses. (a), (b) The cell was able to attach directly to FN fibers with a diameter as small as 1 μm (blue) and establish focal adhesion sites (paxillin = yellow; actin = red), in order to rearrange the regular fiber pattern by applying force from the actin cytoskeleton to the fibrils. Pillar bending, *i.e.*, deflection of the original pillar top positions (white circles), is observed (compare the location of the white circles with the actual pillar top position). (c) Co-localization of paxillin and FN is demonstrated by the ratio images for areas indicated by red and yellow arrows. (d), (e) Thicker bundles, with a diameter of approximately 2 μm, oriented the cell and focal adhesions along the fibril's long axis. In areas where the cell established focal contacts directly with the bundles of fibers, co-localization of FN and paxillin was less apparent (f). Here, deformation was much less dominant than that seen in fibers with diameters smaller than 1 μm.

structural changes, monitored by light microscopy combined with high-resolution SEM, revealed the following structural features:

1. Globular FN particles with an average diameter of *ca.* 32 nm assemble into an insoluble sheet at the air–water interface (Fig. 2e).

2. Application of force to an FN sheet attached to a micropillar array, initially results in the formation of "rough" fibers with globular subdomains (Fig. 2f, g), the dimensions of which are affected by the tension applied to the FN layer. Two major forms of rough fibers were noted, with globular domains measuring either 24 nm (wide) × 16 nm (long) or 19 nm (wide) × 9 nm (long) (Fig. 2f, g).

3. Strongly aligned fibers display a uniform diameter of 14 nm, and smooth surfaces. These are the thinnest FN fibers that we could detect, yet careful examination indicated that they tend to split at their ends into two 7 nm sub-fibrils (Fig. 2h; Fig. 4c). Thicker fibers are formed through lateral aggregation of these 14 nm wide fibers (Fig. 2i).

It should be emphasized that the different particle and fiber morphologies reported herein are based on hrSEM, using both "in-lens" and "secondary electron" modes. This approach enables retrieval of high-resolution data from large specimen areas, yet requires sample dehydration and thin metal coating. While the overall morphology (*e.g.* "smooth" *versus* "rough" fibrils) is readily apparent, analysis of hydrated fibers at finer resolution will be needed, in order to unequivocally correlate the observed morphologies with the degree of locally applied force, or with the degree of FN unfolding.

Furthermore, our data support the concept that the formation of FN fibrils requires application of external forces.[40] The most intriguing question, still unanswered, is the range of force necessary for inducing the various stages in FN unfolding and fibrillogenesis. *In vivo*, such local forces are applied either by the attached cells, or by long-range forces generated elsewhere in the organism. It is noteworthy that cellular contractile forces applied to the FN matrix *via* focal adhesions are within the range of a few tens of nanonewtons.[31,36,41] In our *in vitro* system, a surface tension estimated to be *ca.* 80 mN m^{-1} [33] acts on individual FN particles at the air–solution interface, which is 32 nm in diameter (Fig. 2e). Assuming a linear decrease of surface tension along such a particle, we calculate that a ~2–3 nN force would be necessary, in order to orient and deform particles at the air–solution interface, and drive their lateral aggregation. Upon application of force, the FN sheet, primarily composed of a network of particles, transforms into rough fibers which become smooth and fully stretched when additional force is applied. Data obtained by means of AFM indicate that the range of force needed to cause the unfolding of individual FN molecules is between 5–10 pN.[28,29] In this study, the local forces applied to the FN particles by micropillar bending were estimated by measuring the micropillar displacement, which is within the range of several hundreds of nanonewtons (180 ± 36 nN per pillar). Assuming that this force is equally distributed among the FN particles, each 32 nm in diameter (projected area of $256\pi \times 10^{-18}$ m^2), which are in contact with the pillar plateau (area of $6.25\pi \times 10^{-12}$ m^2) the average force yielded is approximately 8 pN per particle, which is within the range necessary for

FN unfolding. The gradual increase in FN particle stretching (Fig. 4c) leads to the conclusion that forces applied to FN particles in the center of pillar tops are well below 8 pN while forces at the rim are higher. Forces needed for unfolding the compact globular conformation, which is reinforced by electrostatic intra-chain interactions, are less than 5 pN, while forces needed for unfolding FN-III domains are greater than 10 pN.[28,29] The gradual change in structure, observed in Fig. 4c allows us to assume that this force range is generated by the forces applied to FN particles adsorbed to a pillar plateau, thereby enabling observation of the various stages of FN unfolding. Our micromanipulation experiments (Fig. 5) further suggest that FN fibers are highly elastic, in accordance with the literature reporting an elastic elongation of ECM fibers in cell culture of $\Delta l/l_0 = 3.5$[12]. The measured elastic fiber elongation described in this experiment, $\Delta l/l_0 = 0.2$, is considerably lower, due to restricted pillar dimensions and spacing.

As shown in Fig. 2e, FN dimers at the air–liquid interface remained in a globular conformation similar to that reported for globular FN in physiological solution,[38,39] despite the fact that the actual size of the visualized structures was expected to be smaller in dimension, due to dehydration during the processing for hrSEM observations. The partitioning of FN into the interface apparently induces mechanical deformation of the globular FN. Such a force enables adjacent FN molecules to pre-assemble into a stable network, which BSA and IgG molecules fail to do (Fig. 2c, d). This is in agreement with our expectations that FN fiber formation requires proper alignment of the outer FN-I domain, enabling specific intermolecular interactions between the FN-I domains of different chains.[12,42] The regular orientation of the FN molecules, and their close proximity within the 2D sheet, dramatically increase their irreversible aggregation, as shown by FRAP analysis (Fig. 1b). It is also in line with the observation of Baneyx and Vogel, indicating that the interaction of soluble FN with lipid monolayers can induce the assembly of FN fibrils.[21]

Further deformation of the free-hanging FN sheet, resulting from pillar bending, and due to wetting of the microstructure or to direct mechanical manipulation, causes alignment of the globular particle network into rough fibrils consisting of globular domains of *ca.* 24 nm, interspaced by fibrous subunits with a diameter of *ca.* 16 nm (Fig. 1f). Such structural configurations are also observed, occasionally, at apparent "imperfections" in the FN sheet (Fig. 2e, arrow), a finding that further highlights the importance of mechanical deformation either by surface tension at a defect structure, or by pillar bending. The estimated ratio between the width and the length of the fiber subunits (Table 1) is *ca.* 1.5, which is close to the ratio yielded by the dimensions of the elliptical FN molecule in solution, which is *ca.* 1.6.[39] This supports the assumption that the slight deformation and potential orientation of the FN molecule at the air–solution interface leads to a conformation that supports lateral interactions between FN molecules.

Experimental

Contact angle and FRAP measurements

Drops (50 μL) of PBS (Gibco, Grand Island, NY, USA) were placed on glass-bottomed Petri dishes (MatTek, Ashland, MA, USA), coated with a 20 μm thick layer of polydimethylsiloxane (PDMS) (Sylgard 184, Dow Corning Corporation, Midland, MI, USA) with a base-to-cross-linker mixing ratio of 10 : 1. FN or BSA, pre-labeled with Alexa Fluor 565 succinimidyl ester according to manufacturer's instructions (Molecular Probes, Eugene, OR, USA), were injected into the center of the drops, yielding final protein concentrations of 10 or 100 μg mL^{-1}, respectively. Images from the solid–liquid interface were captured at 0.5 s intervals, in order to monitor the protein adsorption at the PDMS surface. At 5, 10 and 20 min after injection, the shape of the drop was imaged by recording a 100 μm thick z-stack; contact angles were then calculated with ImageJ, (version 1.32j). Bleaching of the pre-labeled protein at specific time points was conducted at the air–liquid interface 10 μm above the PDMS surface, using a confocal microscope (Zeiss LSM 5, Pascal, Jena, Germany) equipped with a HeNe and an argon-ion laser at full power. Fluorescence recovery in the bleached area (approx. 5 × 5 μm) was traced over a period of 5 min at 0.5 s intervals, and the values were corrected for photobleaching caused by the repeated scanning. All measurements were performed in a humidified atmosphere to prevent evaporation of the protein solution. Plots were prepared with the Origin software program (v. 7.0, OriginLab, Northampton, MA, USA).

Microarray preparation

Microstructured surfaces were produced by means of standard lithographic techniques.[37] Briefly, a negative replica of the pillars was produced using SU8-10, a standard negative photoresist (Microchemicals GmbH, Berlin, Germany). The lithographic process was performed on a mask aligner (MJB-3, Karl Suess MicroTec Lithography GmbH, Garching, Germany) with a chromium mask written on a Maskwriter (DWL-66, Heidelberg Instruments Mikrotechnik GmbH, Heidelberg, Germany). After preparation of the mold, PDMS was poured over the mold and degassed for 1 h at 5×10^{-2} mbar. The mold was mounted on cover slips (24 × 24 mm, Carl Roth GmbH, Karlsruhe, Germany) and cured at 65 °C for ~12–14 h. A microarray of pillars, each 5 μm in diameter and 10 μm in height, and spaced 4 μm apart, was released by peeling away the mold.

FN fibrillogenesis and immunolabeling

After assembly of the micropillar substrates, 500 μL of PBS aliquots were carefully placed on top of the microarray. The FN solution (1mg mL^{-1} in TBS, Sigma Chemical Co., St. Louis, MO, USA) was then injected into the PBS drop, resulting in a solution with a final FN concentration of 10 or 100 μg mL^{-1}. After 5 min, the samples were rinsed 3 times for 5 min each with 5 mL PBS. Samples were then treated with 0.5% polyvinyl alcohol (PVA, Mowiol 488, Hoechst, Frankfurt, Germany) in PBS to wet the entire microstructure. For time-lapse movies during wetting, a sample was prepared in the same way, using pre-labeled FN or BSA (Sigma) and mounted on an objective slide directly after adding the PVA solution. To visualize the fibrils using epifluorescence microscopy, samples were incubated, without further fixation, with rabbit anti-FN (Sigma) for 1 h, followed by incubation with a fluorescent secondary goat anti-rabbit IgG (Alexa Fluor 488, Molecular Probes). All antibodies were diluted in

0.1% BSA-containing PBS. Cover slips were mounted in PVA (Mowiol 4–88) on objective slides (Carl Roth GmbH) and examined with a Zeiss LSM 5 Pascal using a 63×, 1.4 oil objective.

Single fibril elasticity measurement

To measure the elasticity of FN fibrils associated with the micropillar arrays, labeled FN was applied to the microarray by the injection method previously described, resulting in a final protein concentration of 10μg mL^{-1}. After washing, samples were mounted on a pinched Petri dish to enable observation through the pillars under physiological conditions. To measure the stiffness of single FN fibers, a rigid glass microplate was appended on the tip of a pillar, using a custom-made micromanipulator. By moving the substrate beneath the fixed microplate, the pillar was bent (see also Fig. 4, schematic). Using a Deltavision Spectris System (Applied Precision Inc., Issaquah, WA, USA), consisting of an inverted microscope IX70 equipped with a 60×, 1.2 objective (Olympus, Tokyo, Japan), images were taken after every 100 nm of lateral movement. For elasticity measurements, the sample was moved 1 μm and the stiffness of the analysed pillar (Fig 4; pillar denoted with an asterisk) was set to 0.9 N m^{-1}, corresponding to the height at which the fibers were connected to the sides of the pillar (about 5 μm from the pillar base). Force calculation during the wetting process was performed by analysing the movies with ImageJ software, as described in ref. 37.

Cell culture and electron microscopy

Rat embryo fibroblasts, stably expressing YFP-Paxillin, were cultured in DMEM plus 1% fetal calf serum (Gibco) on the artificially-generated FN fibers for 24 h. For immunofluorescence labeling, cells were fixed, permeabilized with 3% paraformaldehyde (PFA, Merck, Darmstadt, Germany), 0.5% Triton X-100 (Sigma) in PBS for 2 min, and post-fixed with 3% PFA in PBS for 30 min. The cells were then incubated with rabbit anti-FN antibody, and stained with goat anti-rabbit Alexa Fluor 488 antibody, and phalloidin-Tritc (Sigma). Finally, cells were washed with PBS and mounted in Elvanol. Data were acquired with a DeltaVision system (Applied Precision). To investigate cellular FN in greater detail, primary human fibroblasts (HFF, passage 16) were plated on bare silicon wafers (Crystec) in DMEM plus 10% fetal calf serum for 2 or 4 d, and pre-fixed in 3% PFA. After incubation overnight with mouse anti-human FN at 4 °C, and goat anti-mouse IgG conjugated to 15 nm gold particles (EMS, Hatfield, PA, USA) for 2 h at room temperature, cells were post-fixed with 2% glutaraldehyde (EMS) in 0.1 M cacodylate buffer (Merck) for 1 h at room temperature. Membrane-conserving fixation was performed with 1% OsO_4 (EMS) in 0.1M cacodylate buffer for 1h at room temperature. After washing, samples were incubated in a 1% aqueous solution of tannic acid (Merck) for 5 min, and then in 1% aqueous uranyl acetate for 30 min. After washing and dehydration in gradually increasing concentrations of ethanol p.a. (Merck), samples were critically point-dried using CPD30 (BAL-TEC), coated with 2nm Cr using K575X (Emi-Tech, Kent, UK) and visualized in high-resolution SEM Ultra 55 (Zeiss, Oberkochen, Germany). Statistical analysis of particle diameters was performed with ImageJ software.

Conclusions

Our experimental findings support a mechanism for FN fibrillogenesis whereby the two processes proposed by Erickson [12,26] and Vogel [25,27] might occur at distinct, sequential stages of this process. This two-stage process could be activated in our experimental system by varying the level of force applied to FN molecules *via* the micropillars at different stages of fibrillogenesis. Given that FN fibers are indeed elastic, and that their stretching can modulate their strain, we propose that cells fine-tune the biological activity of the underlying matrix by modulating the contractile forces applied *via* their adhesion sites. The force-dependent exposure of new sites on the FN matrix, may, in turn, affect the physiological responses of the cells, including their contractile and signalling activities.

Acknowledgements

We are very grateful to Viola Vogel (ETH Zürich) and Michael Sheetz (Columbia University New York) for enlightening discussions. This study was supported by the Volkswagen-Stiftung and by the National Institutes of Health, through the NIH Roadmap for Medical Research (PN2 EY016586), as well as by the Max Planck Society. Jens Ulmer was supported by a Fellowship from the Minerva Foundation. Benjamin Geiger holds the Erwin Neter Professorial Chair in Cell and Tumor Biology. The overall collaboration between the groups of Benjamin Geiger and Joachim Spatz is strongly supported by the Landesstiftung Baden-Württemberg, within the framework of the program "Spitzenforschung Baden-Württemberg".

References

1 S. Ayad, R. P. Boot-Handford, M. J. Humphries, K. E. Kadler and C. A. Shuttleworth, *The Extracellular Matrix Factsbook*, Academic Press, Elsevier Science Publishing, New York, 1998.
2 V. Vogel and G. Baneyx, *Annu. Rev. Biomed. Eng.*, 2003, **5**, 441–463.
3 A. Katsumi, A. W. Orr, E. Tzima and M. A. Schwartz, *J. Biol. Chem.*, 2004, **279**, 12001–12004.
4 B. Geiger, A. Bershadsky, R. Pankov and K. M. Yamada, *Nat. Rev. Mol. Cell Biol.*, 2001, **2**, 793–805.
5 A. D. Bershadsky, N. Q. Balaban and B. Geiger, *Annu. Rev. Cell Dev. Biol.*, 2003, **19**, 677–695.
6 S. Miyamoto, B. Z. Katz, R. M. Lafrenie and K. M. Yamada, in *Morphogenesis: Cellular Interactions*, 1998, vol. 857, pp. 119–129.
7 D. Guarnieri, S. Battista, A. Borzacchiello, L. Mayol, E. De Rosa, D. R. Keene, L. Muscariello, A. Barbarisi and P. A. Netti, *J. Mater. Sci.: Mater. Med.*, 2007, **18**, 245–253.
8 J. McDonald, *Annu. Rev. Cell Biol.*, 1988, **4**, 183–207.
9 H. Birkedalhansen, W. G. I. Moore, M. K. Bodden, L. J. Windsor, B. Birkedalhansen, A. Decarlo and J. A. Engler, *Crit. Rev. Oral Biol. Med.*, 1993, **4**, 197–250.
10 V. Vogel and M. Sheetz, *Nat. Rev. Mol. Cell Biol.*, 2006, **7**, 265–275.
11 H. P. Erickson, *Proc. Natl. Acad. Sci. U. S. A.*, 1994, **91**, 10114–10118.
12 H. P. Erickson, *J. Muscle Res. Cell Motil.*, 2002, **23**, 575–580.
13 R. Pankov and K. M. Yamada, *J. Cell Sci.*, 2002, **115**, 3861–3863.
14 Y. Mao and J. E. Schwarzbauer, *Matrix Biol.*, 2005, **24**, 389–399.
15 R. O. Hynes, *Fibronectins*, Springer, New York, 1990.
16 J. E. Schwarzbauer and J. L. Sechler, *Curr. Opin. Cell Biol.*, 1999, **11**, 622–627.
17 S. Bourdoulous, G. Orend, D. A. MacKenna, R. Pasqualini and E. Ruoslahti, *J. Cell Biol.*, 1998, **143**, 267–276.
18 F. G. Giancotti and E. Ruoslahti, *Cell*, 1990, **60**, 849–859.

19 J. L. Sechler, H. W. Rao, A. M. Cumiskey, I. Vega-Colon, M. S. Smith, T. Murata and J. E. Schwarzbauer, *J. Cell Biol.*, 2001, **154**, 1081–1088.
20 J. E. Schwarzbauer, *J. Cell Biol.*, 1991, **113**, 1463–1473.
21 G. Baneyx and V. Vogel, *Proc. Natl. Acad. Sci. U. S. A.*, 1999, **96**, 12518–12523.
22 N. L. Halliday and J. J. Tomasek, *Exp. Cell Res.*, 1995, **217**, 109–117.
23 C. Y. Wu, V. M. Keivens, T. E. Otoole, J. A. McDonald and M. H. Ginsberg, *Cell*, 1995, **83**, 715–724.
24 T. Ohashi, D. P. Kiehart and H. P. Erickson, *J. Cell Sci.*, 2002, **115**, 1221–1229.
25 M. L. Smith, D. Gourdon, W. C. Little, K. E. Kubow, R. A. Eguiluz, S. Luna-Morris and V. Vogel, *PLoS Biol.*, 2007, **5**, e268.
26 H. P. Erickson and N. A. Carrell, *J. Biol. Chem.*, 1983, **258**, 4539–4544.
27 G. Baneyx, L. Baugh and V. Vogel, *Proc. Natl. Acad. Sci. U. S. A.*, 2001, **98**, 14464–14468.
28 A. F. Oberhauser, C. Badilla-Fernandez, M. Carrion-Vazquez and J. M. Fernandez, *J. Mol. Biol.*, 2002, **319**, 433–447.
29 M. Rief, M. Gautel and H. E. Gaub, in *Advances in Experimental Medicine and Biology: Elastic Filaments Of The Cell*, ed. H. L. Granzier and G. H. Pollack, Springer, New York, 2000, vol. 481, pp. 129–141.
30 A. Krammer, H. Lu, B. Isralewitz, K. Schulten and V. Vogel, *Proc. Natl. Acad. Sci. U. S. A.*, 1999, **96**, 1351–1356.
31 N. Q. Balaban, U. S. Schwarz, D. Riveline, P. Goichberg, G. Tzur, I. Sabanay, D. Mahalu, S. Safran, A. Bershadsky, L. Addadi and B. Geiger, *Nat. Cell Biol.*, 2001, **3**, 466–472.
32 D. Riveline, E. Zamir, N. Q. Balaban, U. S. Schwarz, T. Ishizaki, S. Narumiya, Z. Kam, B. Geiger and A. D. Bershadsky, *J. Cell Biol.*, 2001, **153**, 1175–1185.
33 J. N. N. Israelachvili, *Intermolecular and Surface Forces*, Academic Press Inc. (London) Ltd, London, 1991.
34 A. Tronin, T. Dubrovsky, S. Dubrovskaya, G. Radicchi and C. Nicolini, *Langmuir*, 1996, **12**, 3272–3275.
35 A. Marmur, *Langmuir*, 2004, **20**, 3517–3519.
36 J. L. Tan, J. Tien, D. M. Pirone, D. S. Gray, K. Bhadriraju and C. S. Chen, *Proc. Natl. Acad. Sci. U. S. A.*, 2003, **100**, 1484–1489.
37 D. H. Zeng, A. Ferrari, J. Ulmer, A. Veligodskiy, P. Fischer, J. Spatz, Y. Ventikos, D. Poulikakos and R. Kroschewski, *Biophys. J.*, 2006, **90**, 4380–4391.
38 D. M. P. Peters, Y. Chen, L. Zardi and S. Brummel, *Microsc. Microanal.*, 1998, **4**, 385–396.
39 B. Sjoberg, M. Eriksson, E. Osterlund, S. Pap and K. Osterlund, *Eur. Biophys. J. Biophy. Lett.*, 1989, **17**, 5–11.
40 G. Baneyx, L. Baugh and V. Vogel, *Proc. Natl. Acad. Sci. U. S. A.*, 2002, **99**, 5139–5143.
41 O. du Roure, A. Saez, A. Buguin, R. H. Austin, P. Chavrier, P. Silberzan and B. Ladoux, *Proc. Natl. Acad. Sci. U. S. A.*, 2005, **102**, 2390–2395.
42 H. H. J. de Jongh, H. A. Kosters, E. Kudryashova, M. B. J. Meinders, D. Trofimova and P. A. Wierenga, *Biopolymers*, 2004, **74**, 131–135.